

Quaternary Structure of Coronavirus Spikes in Complex with Carcinoembryonic Antigen-related Cell Adhesion Molecule Cellular Receptors*

Received for publication, February 25, 2002
Published, JBC Papers in Press, March 23, 2002, DOI 10.1074/jbc.M201837200

Daniel N. Lewicki and Thomas M. Gallagher‡

From the Department of Microbiology and Immunology, Loyola University Medical Center, Maywood, Illinois 60153

Oligomeric spike (S) glycoproteins extend from coronavirus membranes. These integral membrane proteins assemble within the endoplasmic reticulum of infected cells and are subsequently endoproteolyzed in the Golgi, generating noncovalently associated S1 and S2 fragments. Once on the surface of infected cells and virions, peripheral S1 fragments bind carcinoembryonic antigen-related cell adhesion molecule (CEACAM) receptors, and this triggers membrane fusion reactions mediated by integral membrane S2 fragments. We focused on the quaternary structure of S and its interaction with CEACAMs. We discovered that soluble S1 fragments were dimers and that CEACAM binding was entirely dependent on this quaternary structure. However, two differentially tagged CEACAMs could not co-precipitate with the S dimers, suggesting that binding sites were closely juxtaposed in the dimer (steric hindrance) or that a single CEACAM generated global conformational changes that precluded additional interactions (negative cooperativity). CEACAM binding did indeed alter S1 conformations, generating alternative disulfide linkages that were revealed on SDS gels. CEACAM binding also induced separation of S1 and S2. Differentially tagged S2 fragments that were free of S1 dimers were not co-precipitated, suggesting that S1 harbored the primary oligomerization determinants. We discuss the distinctions between the S-CEACAM interaction and other virus-receptor complexes involved in receptor-triggered entry.

For enveloped viruses, efficient infection requires a regulated coalescence of virion and cellular membranes. Temporal and spatial regulation of this membrane fusion event must occur for viral genomes to enter into a milieu suitable for subsequent replicative processes. Protruding virion glycoproteins, each poised to induce membrane coalescence, have therefore evolved sensitivities to the environmental conditions found at entry sites. These conditions trigger coordinated and irreversible changes in virion glycoprotein conformations that can culminate in membrane fusion. Well known triggers for conformational change include cellular receptor binding (1–4) and/or the low pH exposures that occur following engulfment of virus particles into endosomes (5–7).

* This work was supported in part by National Institutes of Health Grant R01 NS 31616 (to T. M. G.) and NIAID Grant 5 T32 AI07508-05 from the National Institutes of Health (to K. L. Knight). The costs of publication of this article were defrayed in part by the payment of page charges. This article must therefore be hereby marked "advertisement" in accordance with 18 U.S.C. Section 1734 solely to indicate this fact.

‡ To whom correspondence should be addressed: Dept. of Microbiology and Immunology, Loyola University Medical Center, 2160 South First Ave., Maywood, IL 60153. Tel.: 708-216-4850; Fax: 708-216-9574; E-mail: tgallag@lumc.edu.

Our studies have focused on murine hepatitis coronavirus (MHV)¹ as a model for understanding receptor-triggered entry processes. This virus is a well studied prototype member of the Coronaviridae, plus-strand RNA viruses that cause a wide range of diseases in humans and animals (8). Because the distinct species specificity and tissue tropism of coronavirus strains largely correlate with changes in the spike (S) protein (9–11), details about S interactions with receptors can enhance our understanding of pathogenesis.

S proteins are classical type I membrane proteins, with ~1300 residue ectodomains, 18-residue transmembrane spans, and a 38-residue cytoplasmic tail (12). Oligomerization occurs rapidly after synthesis (13) and is followed by transport through the exocytic pathway. Within the trans-Golgi network, a furin-like protease cleaves the full-length spike into two similar-sized fragments, a peripheral S1, and a membrane-anchored S2 (14, 15). S1, which associates with S2 through noncovalent interactions, is responsible for binding to cellular receptors. S2 contains the core machinery necessary for membrane fusion (16).

Receptors for the MHV S proteins include numerous members of the carcinoembryonic antigen-related cell adhesion molecule (CEACAM) family, immunoglobulin-like glycoproteins that serve as entry portals for a relatively wide variety of pathogens (17–21). The prototype receptor for MHV, murine CEACAM isoform 1^a, is a type I transmembrane glycoprotein with four Ig-like ectodomains designated as N (amino-terminal)-A1^a-B^a-A2^a (22). The N-domain binds to S proteins (17). After binding to a soluble N-CEACAM fragment, spikes undergo a conformational change that can, in some cases, be revealed as S1 shedding from S2 (23). This structural change may be relevant to MHV entry, as S1 separation from S2 correlates with increased membrane fusion activity (23). A conservative view is that the CEACAM binding to S releases free energy that drives the conformational changes required to promote coalescence of the virus and cell membranes. Indeed, soluble forms of CEACAM can, through binding S proteins, increase the propensity of S to fuse membranes (24).

Understanding the connections between CEACAM binding and membrane fusion depends in part on a view of the actual CEACAM-binding site(s) on the S protein. Kubo *et al.* (25) mapped the CEACAM-binding sites to the amino-terminal 330 residues of S1, but high resolution protein structures are cur-

¹ The abbreviations used are: MHV, murine hepatitis virus; CEACAM, carcinoembryonic antigen-related cell adhesion molecule; DMEM, Dulbecco's modified Eagle's medium; FCS, fetal calf serum; TK, thymidine kinase; DPR, deletion prone region; PBS, phosphate-buffered saline; mAb, monoclonal antibody; β -ME, β -mercaptoethanol; EGFP, enhanced green fluorescent protein; HRPO, horseradish peroxidase; DSP, dithiobis(succinimidylpropionate); NEM, N-ethylmaleimide; gp, glycoprotein.

rently unknown. Questions also remain concerning quaternary structures, both S dimers and trimers have been proposed (13, 26). Thus, we embarked on studies assessing the oligomeric organization of S and S-CEACAM complexes.

Here we report that S1, when shed from S2 or when produced independently from cDNAs, exists stably as a dimer. We discovered that S1 dimers, but not monomers, will bind to CEACAM receptors. In fact, we found that the region conferring dimerization resides at or near the CEACAM1^a-binding site, an unexpected finding because oligomerization determinants in functionally analogous spike proteins of other viruses reside within the integral membrane fragments (27–35). Remarkably, only one CEACAM bound each S1 dimer, and we identified a novel disulfide-linked S1 conformation in S1-CEACAM complexes. Our findings refine the current understanding of CEACAM receptors as mediators of conformational change, and they form the basis for a preliminary model of receptor-triggered entry with both parallels and deviations from established paradigms for enveloped virus entry (36–41).

EXPERIMENTAL PROCEDURES

Cells—HeLa-tTA and rabbit kidney clone 13 (RK13) cells were grown in Dulbecco's modified Eagle's medium (DMEM) supplemented with 10% heat-inactivated fetal calf serum (FCS). 293 EBNA cells secreting N-CEACAM_{Fc} (formerly known as sMHRV-Ig) (42) were grown in DMEM, 10% FCS containing the antibiotics G418 (100 μg/ml) and hygromycin B (200 μg/ml).

Mutagenesis of CEACAM and Spike cDNAs—We used murine CEACAM1^a cDNA (22, 42) as template for PCR amplification of N-CEACAM_{6×His}, using the primer 5' GTCGAGTCAGTGGTGGTGGTGGTGGTGTACATGAAATCG 3', which encodes a hexahistidine tag. We used cDNA of S (strain JHM) (43) as a template for PCR amplification of S gene and truncated S fragments. To create S_{T212S/Y214S/Y216S}, mutagenic oligonucleotides 5' GGTGGTCTTTTCTGCGTCTATGCGGAT 3' and its complement were used in PCRs. To generate enhanced green fluorescent protein (EGFP)-tagged spikes, we engineered pTM1-S (42) with a unique *NotI* restriction site using the following oligonucleotide: 5' GGGCTCGAGTCAGCGCCGCTCACAGGGATCCAGTGCATCCTCATGGGC 3'. EGFP DNA was PCR-amplified from pEGFP (Clontech), and 741-nucleotide *NotI/BamHI* restriction fragment was cloned into the aforementioned pTM1-S_(NotI).

Mutations in the CEACAM and S genes were confirmed by DNA sequencing. Restriction fragment exchanges with the vaccinia virus insertion-expression vector pTM1-S and pTM3-S1 were all performed as described previously (42). All recombinant plasmids were cloned and amplified in *E. coli* DH5α (for pTM1 vector) or HB101 (for pTM3 vector). Plasmids pTM1-S_{ΔDPR2} (23) and pTM1-S_{EGFP} were used directly, without recombination into vaccinia vectors. The S_{EGFP} protein includes the entire S_{ΔDPR2} followed by an eight-residue linker (ALDPPVAT) and a C-terminal 238-residue EGFP.

Generation of Recombinant Vaccinia Viruses—Plasmids were recombined into the thymidine kinase (TK) gene of vaccinia virus (strain WR) by standard methods (44), and TK-negative virus isolates were amplified in RK13 cells. TK-negative virus stocks were screened for S or CEACAM cDNA expression by co-infection with vTF7.3 (45) and immunoblot detection of the respective proteins in cell lysates, as described previously (23). We used the following vaccinia recombinants: vTM3-S1 (encodes 769-residue S1 of JHM strain); vTM3-S1₃₃₀ (encodes 330-residue amino-terminal S1 fragment); vTM3-S1_{ΔDPR1} (encodes S1 with internal deletion of residues 446–598); vTM3-S1_{ΔDPR2} (encodes S1 with internal deletion of residues 429–586); vTM1-S_{E_{CTO}} (encodes 1320 residue S1/S2 lacking transmembrane span and cytoplasmic tail); vTM1-S_{T212S/Y214S/Y216S} (encodes full-length S of JHM strain with the indicated substitutions); vTM3-CEACAM_{E_{CTO}} (encodes N-A1-B-A2 Ig-like domains of CEACAM); vTM3-N-CEACAM_{6×His} (encodes N-domain of CEACAM with 6 carboxyl-terminal histidines).

Preparation of Soluble CEACAM and Spike Proteins—To obtain N-CEACAM_{Fc}, 293 EBNA:N-CEACAM_{Fc} cells (42) were incubated overnight in serum-free DMEM. Culture supernatant was collected, filtered through a 0.22-μm membrane, dialyzed against PBS-P (PBS (pH 7.4) containing 0.01% protease inhibitor mixture (Sigma)), and concentrated 100-fold by ultrafiltration. In some cases, N-CEACAM_{Fc} was further purified by affinity chromatography on Sepharose-protein G (Amersham Biosciences). Supernatants typically yielded ~2 μg of N-CEACAM_{Fc} per ml.

To obtain ³⁵S-labeled recombinant S proteins and CEACAM_{E_{CTO}}, monolayers of HeLa-tTA cells were inoculated at 2 plaque-forming units/cell for 1 h at 37 °C with vTF7.3 and the respective recombinant vaccinia viruses. At 6 h post-infection, the medium was replaced with labeling media (DMEM, 1% dialyzed FCS lacking cysteine and methionine). After 1 h, the labeling media was replaced with serum-free labeling media supplemented with 25 μCi/ml Tran³⁵S-label (ICN). After a 5-h incubation, the harvested media were clarified by centrifugation, dialyzed, and concentrated ~100-fold by ultrafiltration as described above.

Immunoprecipitations—S proteins were collected from media or from cytoplasmic extracts. Extracts were obtained by lysing infected cell monolayers with PBS-P containing 0.5% Nonidet P-40, followed by removal of nuclei by centrifugation at 3000 × g for 15 min. S proteins were immunoprecipitated with N-CEACAM_{Fc}, with polyclonal anti-JHM serum (R33 serum, a gift from Dr. Stanley Perlman, University of Iowa), or with monoclonal anti-S antibody J.2.6 (J.2.6 hybridoma (46), a gift from Dr. John Fleming, University of Wisconsin, Madison) or with monoclonal anti-S antibody number 2 (a gift from Dr. Fumihiko Taguchi, National Institute of Neuroscience, Tokyo, Japan). Briefly, these Igs were bound for 4 h at 4 °C to Gamma Bind G-Sepharose beads (Amersham Biosciences). The beads were then rinsed three times with PBS-P by centrifugation and resuspension. After overnight incubation at 4 °C with media or cytoplasmic extracts, beads were rinsed by five cycles of centrifugation and resuspension with PBS-P containing 0.5% Nonidet P-40. The final bead pellets were mixed with SDS solubilizer (2% SDS, 5% β-mercaptoethanol (β-ME), 2.5% Ficoll, 0.005% bromophenol blue) for 5 min at 100 °C. Dissolved proteins were then visualized after SDS-PAGE by fluorography or immunoblotting, as described previously (23).

Velocity Gradient Ultracentrifugation—Samples containing ³⁵S-labeled S1 or S1-CEACAM complexes were overlaid onto linear 5 ml of 5–20% w/w sucrose gradients in PBS-P containing 0.01% BSA. A parallel gradient was overlaid with an extract containing the sedimentation markers horseradish peroxidase (HRPO 4 S), human immunoglobulin G1 (IgG 7 S), and *E. coli* β-galactosidase (16 S). After sedimentation at 55,000 rpm at 5 °C for 5.95 h in a Beckman Spinco SW55 rotor, fractions (20 per gradient) were collected. The S proteins in gradient fractions were then immunoprecipitated and visualized by fluorography after SDS-PAGE. Sedimentation standards were identified in the fractions by enzymatic assays (HRPO by turnover of 2,2'-azino-bis(3-ethylbenzthiazoline-6-sulfonic acid substrate; IgG by immunoblotting with goat anti-human IgG:alkaline phosphatase; β-galactosidase by turnover of chlorophenol red-β-D-galactopyranoside substrate).

Cross-linking of Oligomeric Spikes—Dithiobis(succinimidylpropionate) (DSP) (25 mM in dimethyl sulfoxide) was added at various dilutions to ³⁵S-labeled S1 in PBS (pH 7.4). After 30 min at 22 °C, reactions were quenched with 50 mM Tris-HCl (pH 7.0). The ³⁵S-labeled S1 proteins were then immunoprecipitated with N-CEACAM_{Fc}, eluted with SDS solubilizer lacking β-ME, electrophoresed on a 4–20% polyacrylamide gradient gel under reducing and non-reducing conditions, and then visualized via fluorography.

Co-production and Immunoprecipitation of S2 and S2_{EGFP}—vTF7.3-infected HeLa-tTA cells were lipofected with pTM1-S and with pTM1-S_{EGFP}, alone or together, using LipofectAMINE PLUS according to manufacturer's instructions (Invitrogen). At 4 h post-lipofection, media were removed and replaced for 1 h with labeling media and then 5 h with labeling media containing 25 μCi/ml Tran³⁵S-label. Cell monolayers were lysed with PBS-P (pH 8.5) containing 0.5% Nonidet P-40, and nuclei were pelleted by centrifugation (3000 × g for 10 min at 4 °C).

To separate ³⁵S-labeled S1 from S2, leaving S1 associated with Sepharose beads, ³⁵S-labeled S proteins in clarified cytoplasmic extracts were captured by incubation for 4 h at 4 °C with Sepharose G:N-CEACAM_{Fc} beads, and suspensions were incubated for an additional 4 h at 37 °C before pelleting beads (3000 × g for 10 min at 4 °C). Supernatants enriched in S2 were further depleted of residual S1 by two additional cycles of incubation with fresh Sepharose G:N-CEACAM_{Fc} beads. The final supernatants were then incubated overnight at 4 °C with Sepharose G:anti-GFP antiserum to capture S2_{EGFP} fragments. Beads were rinsed extensively with PBS-P containing 0.5% Nonidet P-40, suspended in SDS solubilizer, and heated to 100 °C for 5 min. Dissolved proteins were visualized by immunoblot with anti-S2 mAb 10G (a gift from Drs. Stuart Siddell and Fumihiko Taguchi) (47) after SDS-PAGE. Fluorograms of immunoblots were obtained using a Molecular Dynamics Typhoon 8600 PhosphorImager.

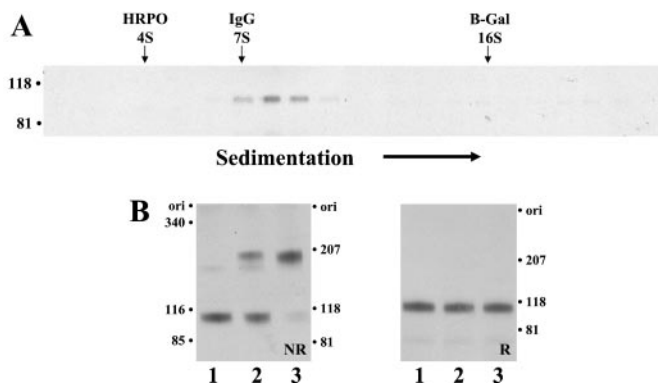


FIG. 1. Biochemical analysis of S1 quaternary structure. A, recombinant ^{35}S -labeled S1 (strain JHM) was sedimented on a linear 5–20% sucrose gradient, and the ^{35}S -labeled S1 in gradient fractions was visualized after immunoprecipitation onto Sepharose G:N-CEACAM_{Fc} beads, SDS-PAGE, and fluorography. The positions of standards horseradish peroxidase (HRPO 4S), human IgG1 (IgG 7S), and β -galactosidase (β -Gal 16S) are indicated above the electropherogram. B, recombinant ^{35}S -labeled S1 was incubated at room temperature for 30 min with 0 (lane 1), 0.08 mM (lane 2), or 0.25 mM DSP (lane 3) and then immunoprecipitated onto Sepharose G:N-CEACAM_{Fc} beads and visualized via fluorography following SDS-PAGE on a 4–20% acrylamide gradient gel under non-reducing (NR) and reducing (R) conditions.

RESULTS

Peripheral S1 Fragments Are Dimers—It is still unclear whether coronavirus peplomers are dimers or trimers. Venema *et al.* (13) reported that MHV spikes are dimers, and Delmas and Laude (26) provided evidence for cross-linking of transmissible gastroenteritis coronavirus spikes into trimers. Noting the importance of quaternary structure in viral glycoprotein function, we decided to return to the question of S protein oligomerization in the MHV system. We initially used velocity gradient ultracentrifugation and chemical cross-linking to determine the quaternary structure of peripheral S1 fragments. We found that S1 produced independently from cDNA sedimented to an ~ 9 S position on sucrose gradients (Fig. 1A). Identical results were obtained for S1 fragments that had separated from S2 (data not shown). Formulas based on isokinetic sedimentation of globular proteins indicated that the ~ 9 S material would have a molecular mass of ~ 200 kDa, consistent with S1 homodimers (48). However, elongated molecules like the coronavirus spike peplomer (49) might exhibit unusual sedimentation behavior in sucrose gradients; therefore, we further addressed quaternary structure by cross-linking ^{35}S -labeled S1 with DSP, a thiol-cleavable chemical cross-linker. Cross-linked spikes were then immunoprecipitated and electrophoresed under non-reducing and reducing conditions (Fig. 1B). S1 dimers appeared with increasing concentrations of DSP, and β -ME reduced these dimers into monomers. Extraordinarily high DSP concentrations (25 mM) did not complex ^{35}S -labeled S1 into higher order oligomers (data not shown).

CEACAM Receptor-binding Sites Are Only Present in S Oligomers—In previous experiments, we found that polyclonal anti-spike antibodies captured newly synthesized ^{35}S -labeled S proteins, whereas N-CEACAM_{Fc}, an immunoadhesion consisting of the N-domain of murine CEACAM1^a linked to a carboxyl-terminal IgG1 Fc, did not. The ^{35}S -labeled spikes bound N-CEACAM_{Fc} only after ~ 30 min of maturation (23). One possible explanation for this finding was that S proteins oligomerized during the 30-min maturation process and that soluble receptors only recognized oligomers. This contention was consistent with numerous reports that glycoprotein oligomerization is required to maintain native tertiary structures (50, 51). Therefore, we separated newly synthesized spikes by rate-

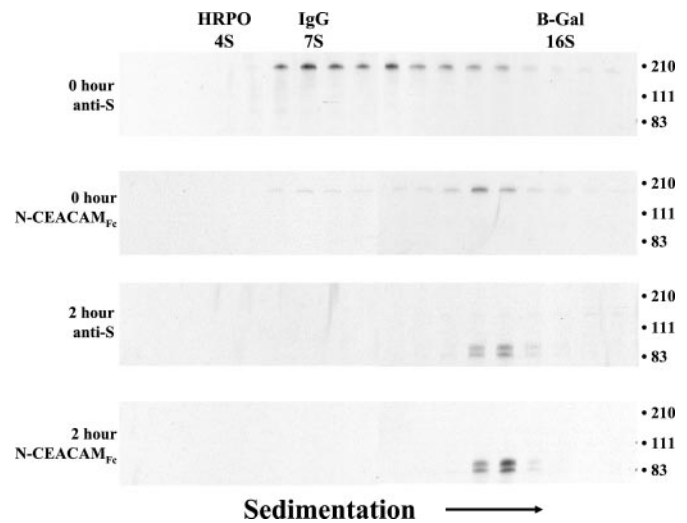


FIG. 2. Specific capture of assembled S oligomers by N-CEACAM_{Fc}. HeLa cells synthesizing S proteins were pulse-labeled with Tran ^{35}S -label for 30 min and either lysed immediately (0 hour) or chased for 2 h at 37 °C before lysis (2 hour). Lysates were sedimented on sucrose gradients, and S proteins in each fraction were immunoprecipitated with polyclonal antiserum (anti-S) or with N-CEACAM_{Fc} (N-CEACAM_{Fc}) before SDS-PAGE and visualization by fluorography. The sedimentation markers horseradish peroxidase (HRPO 4S), immunoglobulin G (IgG 7S), and β -galactosidase (B-Gal 16S) were identified in fractions from a parallel gradient by enzyme or immunodetection assays, and their positions are indicated above the electropherograms.

zonal sedimentation through sucrose gradients prior to immunoprecipitation and detection on SDS-polyacrylamide gels. Polyclonal anti-spike serum captured a range of spike forms from ~ 6 S to ~ 14 S (Fig. 2, 0 hour anti-S). In contrast, N-CEACAM_{Fc} specifically immunoprecipitated ~ 14 S macromolecules (Fig. 2, 0 hour N-CEACAM_{Fc}). When a 2-h chase period occurred prior to cell lysis and sedimentation, N-CEACAM_{Fc} and anti-S antiserum captured only the ~ 14 S forms (Fig. 2, 2 hour panels). The two endoproteolytic cleavage products S1 (lower band) and S2 (upper band) indicated that most of the spikes had encountered a trans-Golgi-localized furin-like protease (14). These findings indicate that newly synthesized S proteins form CEACAM-binding sites concomitant with their oligomerization.

We next considered whether CEACAM-binding sites disappeared when S proteins dissociated into monomers. We could address this question because our S1 preparations moderately break down when incubated for 2 h at 37 °C. On sucrose gradient sedimentation, the 37 °C-treated S1 occupied two positions, ~ 9 S and ~ 6 S, with ~ 6 S being consistent with 110-kilodalton monomers (48) (Fig. 3, top panel). N-CEACAM_{Fc} only precipitated the ~ 9 S material (Fig. 3, bottom panel), suggesting that monomers do not contain a CEACAM-binding site. Interestingly, soluble ectodomain fragments of S2 co-sedimented with the ~ 6 S S1 monomers in these gradients.

The Extreme Amino-terminal Portion of the Spike Participates in Oligomerization—Although many viral glycoproteins oligomerize through associations between integral membrane fragments (27–35), the MHV S proteins formed dimers of peripheral S1 fragments. To delineate further the sites on S1 responsible for oligomer formation, we took advantage of the discoveries of Kubo *et al.* (25), who determined that the amino-terminal 330 residues of S1 (S1₃₃₀) can independently form a receptor-binding site. If the receptor-binding site requires oligomerization (Fig. 2, 0 hour N-CEACAM_{Fc} panel), then S1₃₃₀ might be a homodimer. If so, S1₃₃₀ fragments would form hetero-oligomeric complexes with larger, complete S1 fragments (S1₇₆₉) in cells concomitantly synthesizing both polypeptides.

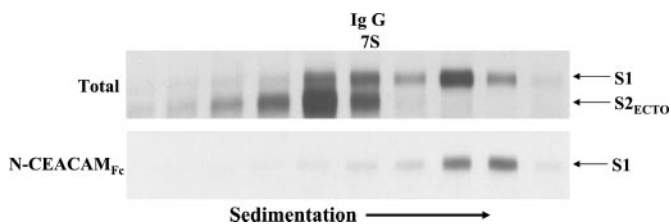


FIG. 3. Influence of S1 quaternary structure on its ability to bind CEACAM. ^{35}S -Labeled S_{ECTO} in sucrose gradient fractions was precipitated with trichloroacetic acid (*top panel*) or with N-CEACAM $_{\text{Fc}}$ (*bottom panel*) and then detected by fluorography following SDS-PAGE. The sedimentation marker immunoglobulin G (*IgG 7S*) was identified in fractions from a parallel gradient by immunodetection assays, and its position is indicated *above* the electropherogram. The positions of S1 and $\text{S}_{2_{\text{ECTO}}}$ are also indicated.

We synthesized recombinant S_{1769} and S_{1330} in HeLa cells, alone or together, using vaccinia vectors. After 2-h radiolabeling periods with Tran ^{35}S -label, we lysed the cell monolayers and immunoprecipitated the S_{1769} with an anti-spike mAb (J.2.6) (46). The mAb J.2.6, whose epitope we roughly mapped to residues 510–540,² should only directly precipitate the S_{1769} fragment. In contrast, N-CEACAM $_{\text{Fc}}$ would precipitate both S_{1769} and S_{1330} proteins.

Indeed, N-CEACAM $_{\text{Fc}}$ recognized and precipitated both the independently produced S_{1769} and S_{1330} fragments from the media and cytoplasmic extracts (Fig. 4). As expected, mAb J.2.6 recognized the S_{1769} fragment but did not precipitate the independently produced S_{1330} fragment. However, mAb J.2.6 precipitated both fragments when they were co-synthesized, indicating hetero-oligomers (Fig. 4, *lane 8, lower panel*, arrow). Unlike the homo-oligomers, cells did not secrete $\text{S}_{1769}\text{S}_{1330}$ hetero-oligomers (Fig. 4, *lane 8, upper panel*), which we interpret as a failure to adopt native glycoprotein structure in the endoplasmic reticulum (50, 52).

Each S Dimer Binds One CEACAM Molecule—Because receptors can perform an essential role in reorganizing viral spikes into structures that can mediate membrane fusion (2–4,53), we sought further details on S-CEACAM interactions. Our data indicated that relatively small S fragments bound CEACAM receptors only when combined into dimers. However, it remained uncertain whether multiple receptors could coordinately bind a single S1 dimer. We addressed this question initially by sedimenting $\text{S1}\cdot\text{N-CEACAM}_{\text{Fc}}$ complexes on sucrose gradients. If each S1 monomer contained a separate CEACAM-binding site, then two dimers might link to the bivalent N-CEACAM $_{\text{Fc}}$ to form an estimated 16 S complex (48). Higher order complexes also may form at equivalent $\text{S1}\cdot\text{N-CEACAM}_{\text{Fc}}$ ratios. However, we observed only ~ 16 S complexes and no evidence of higher order aggregates (Fig. 5).

We obtained additional insight into the stoichiometry of $\text{S1}\cdot\text{N-CEACAM}_{\text{Fc}}$ complexes by co-producing both ligands in 293 cells in the presence of Tran ^{35}S -label, ensuring that the synthesis of S1 exceeded that of N-CEACAM $_{\text{Fc}}$. From the radioactive media, we then precipitated ^{35}S -labeled N-CEACAM $_{\text{Fc}}$ in complex with ^{35}S -labeled S1 using Sepharose-protein G beads. After electrophoretic separation of the precipitated proteins, we determined ^{35}S -labeled $\text{S1}\cdot^{35}\text{S}$ -labeled N-CEACAM $_{\text{Fc}}$ ratios of 3.40 ± 0.05 ($n = 3$). Complexes in which one S1 dimer is tethered to each arm of the bivalent N-CEACAM $_{\text{Fc}}$ (Fig. 5A) would be expected to have an ^{35}S -labeled $\text{S1}\cdot^{35}\text{S}$ -labeled N-CEACAM $_{\text{Fc}}$ ratio of 3.428 (42, 43).

We next used a series of co-immunoprecipitation tests to further address whether more than one CEACAM could simultaneously bind an S oligomer. A soluble CEACAM bound to S1

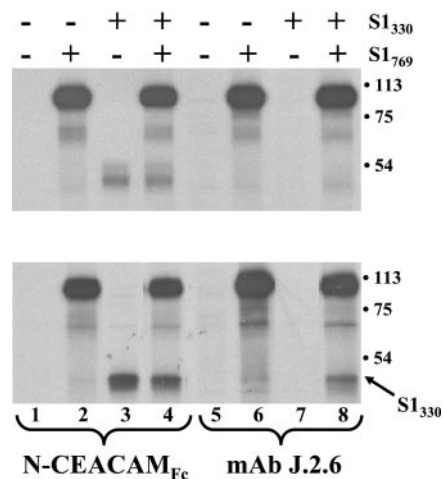


FIG. 4. Co-immunoprecipitation of amino-terminal fragments S_{1330} and S_{1769} . Recombinant S1 fragments of 330 or 769 residues were synthesized alone or together in HeLa cells in the presence of Tran ^{35}S -label. S fragments in the media (*top panel*) and cell lysates (*bottom panel*) were immunoprecipitated with N-CEACAM $_{\text{Fc}}$ or with anti-spike mAb J.2.6. The J.2.6 epitope is between S1 residues 510 and 540. ^{35}S -Labeled proteins were visualized by fluorography following SDS-PAGE.

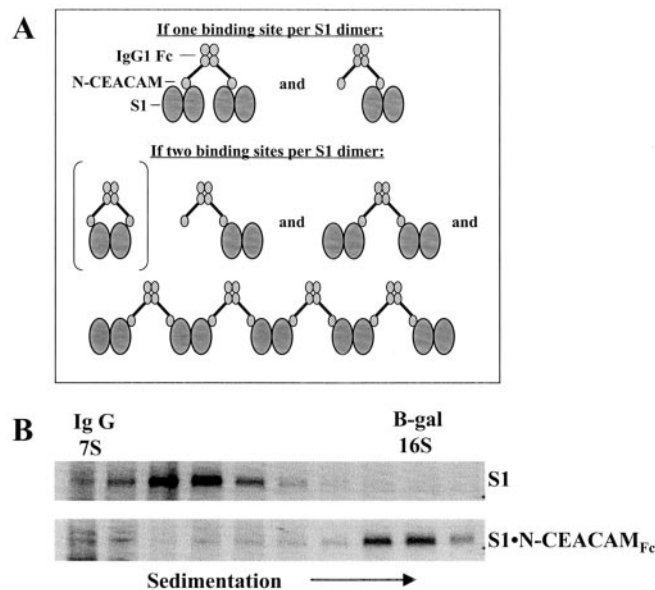


FIG. 5. Sucrose gradient sedimentation analysis of unbound S1 and $\text{S1}\cdot\text{N-CEACAM}_{\text{Fc}}$ complexes. A, two possibilities for the CEACAM-binding site architecture on a S1 dimer are illustrated. If only one CEACAM binds each S1 dimer, then divalent N-CEACAM $_{\text{Fc}}$ would bind one or two S1 dimers. Alternatively, two CEACAM-binding sites could complex S1 and N-CEACAM $_{\text{Fc}}$ into higher order oligomers. B, unbound ^{35}S -labeled S1 and ^{35}S -labeled $\text{S1}\cdot\text{N-CEACAM}_{\text{Fc}}$ complexes were sedimented on linear sucrose gradients and detected in gradient fractions after immunoprecipitation, SDS-PAGE, and fluorography. The sedimentation markers immunoglobulin G (*IgG 7S*) and β -galactosidase (*B-gal 16S*) were identified in fractions from a parallel gradient by enzyme or immunodetection assays, and their positions are indicated *above* the electropherograms. An ~ 16 S $\text{S1}\cdot\text{N-CEACAM}_{\text{Fc}}$ complex was identified. There was no evidence of larger complexes in pellet fractions (not shown).

may or may not prevent the subsequent binding of another alternatively tagged (and thus distinguishable) soluble receptor. We bound recombinant S1 dimers to ^{35}S -labeled CEACAM $_{\text{ECTO}}$, which contains the four ectodomain fragments (N-A1-B-A2) of murine CEACAM1^a (17, 22). We then immunoprecipitated these complexes with N-CEACAM $_{\text{Fc}}$, which possesses the unique, easily captured, Fc tag. Immunoprecipi-

² T. M. Gallagher, unpublished observations.

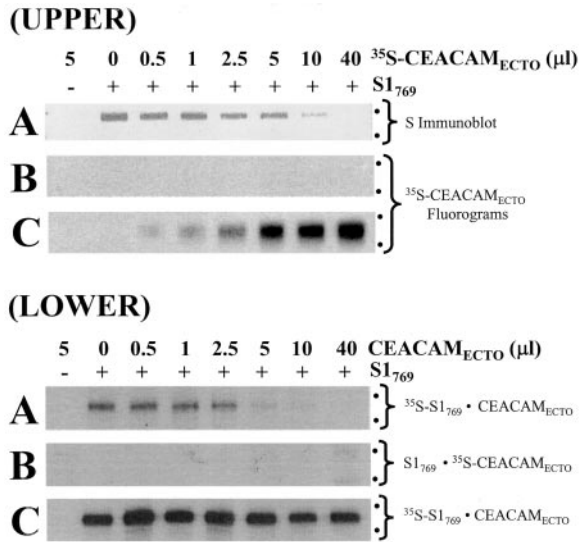


FIG. 6. Immunoprecipitation of S1-CEACAM complexes. *Upper*, constant amounts of recombinant S1 were incubated with increasing quantities of ^{35}S -labeled CEACAM_{ECTO} for 12 h at 4 °C, and proteins in each aliquot were then immunoprecipitated with immobilized N-CEACAM_{Fc} (A and B) or immobilized anti-spike mAb J.2.6 (C). (*Lower*). Constant amounts of recombinant S1 (^{35}S -labeled as indicated) were incubated with increasing amounts of CEACAM_{ECTO} (^{35}S -labeled as indicated) for 12 h at 4 °C, and proteins were then affinity-purified with N-CEACAM_{6×His} (A and B) or immunoprecipitated with mAb J.2.6 (C). The dots on the right of each panel represent the positions of the 113- and 75-kDa molecular mass markers.

tation of the ^{35}S -labeled CEACAM_{ECTO} would indicate that both receptors bound simultaneously to S1 dimers. This receptor-binding state would be consistent with an S oligomer whose structure parallels those of influenza hemagglutinin and HIV gp120, in which each monomer (of the trimer) can bind a single cell-surface ligand (27, 54).

In these assays, N-CEACAM_{Fc} did not precipitate ^{35}S -labeled CEACAM_{ECTO} fragments over a range of S1: ^{35}S -labeled CEACAM ratios (Fig. 6, *Upper*, B). Anti-S1 (mAb J.2.6) precipitations showed that ^{35}S -labeled CEACAMs indeed complexed with S1 at subsaturating levels (Fig. 6, *Upper*, C). We also observed diminished immunoprecipitation of S proteins by N-CEACAM_{Fc} as CEACAM_{ECTO} concentrations increased, again supporting the contention that the two different receptors could not concomitantly bind S1 dimers (Fig. 6, *Upper*, A).

We considered the possibility that the large carboxyl-terminal Fc “tags” might cause an “artificial” steric hindrance in these tests. Thus, in parallel co-precipitation tests, we replaced N-CEACAM_{Fc} with N-CEACAM_{6×His}, whose 6-residue appendage is roughly 100 times smaller than IgG Fc. N-CEACAM_{6×His} also could not precipitate S1: ^{35}S -labeled CEACAM_{ECTO} complexes (Fig. 6, *Lower*, B), but it could readily bind and precipitate free S1 dimers (Fig. 6, *Lower*, A). Thus, for steric hindrance to account for this interference by CEACAM_{ECTO}, separate binding sites on each S1 monomer would have to be very closely juxtaposed in the dimer.

We also considered the unconventional possibility that an S1 dimer contains only a single asymmetric binding site for CEACAM that is formed by different residues contributed by each S1 monomer. We synthesized S1 proteins with the changes T212S, Y214S and Y216S, which Suzuki and Taguchi (55) had shown to decrease CEACAM binding. We found that N-CEACAM_{Fc} inefficiently precipitated this mutant, but its capture increased 2-fold when hetero-oligomerized with wild-type S₃₃₀ (Fig. 7 boxed bands). These results argue for a traditional view, in which each S1 monomer (in the context of a dimer) contains a complete CEACAM-binding site.

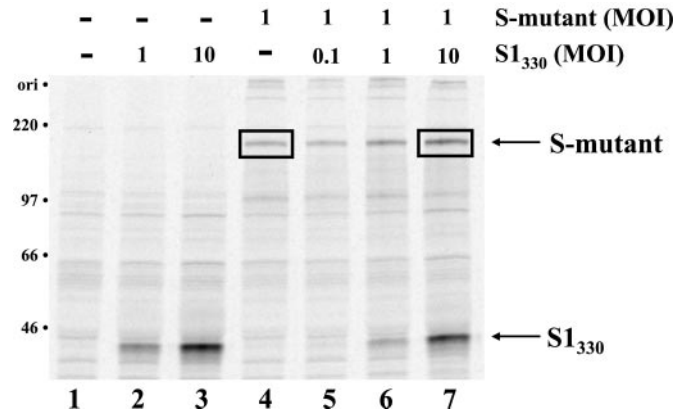


FIG. 7. Increased capture of mutant S proteins with low affinity CEACAM-binding sites by heteromerization with S1₃₃₀ fragments. Recombinant mutant S proteins with three point mutations within the CEACAM-binding site were synthesized alone or with increasing amounts of “wild-type” S1₃₃₀. S1₃₃₀ synthesis was adjusted by the input multiplicity of infection (MOI) of the vTM3-S1₃₃₀ vector. ^{35}S -labeled spikes were immunoprecipitated with N-CEACAM_{Fc} and visualized by fluorography following SDS-PAGE. The amount of ^{35}S associated with the boxed bands was quantitated with a Molecular Dynamics Typhoon 8600 PhosphorImager. The left box contained 2141 cpm and the right box contained 4329 cpm.

A CEACAM-induced Conformational Change of S1—Our data suggested that each monomer of the S1 dimer contained an independent CEACAM-binding site. Although sterically hindered sites might explain how only one CEACAM binds S1 oligomers, another possibility was negative cooperativity. For negative cooperativity to be a viable possibility, CEACAM would have to bind one S1 monomer (of the dimer) and induce structural rearrangements such that the adjacent monomer would have substantially reduced CEACAM affinity. Thus, we evaluated whether CEACAM binding induces structural rearrangements in S1.

On considering possible assays for structural rearrangements, we noted that reduction strongly affects the electrophoretic mobility of some variant S1 fragments, ~70 and 90 kDa before and after β -ME treatment, respectively. Thus we entertained the possibility that CEACAM binding might induce conformational changes that rearrange complex disulfide architectures, thereby creating electrophoretic mobility shifts. It is important to note that we felt any positive results might even have some biological relevance, as we had shown earlier (56) that chemicals preventing disulfide rearrangements block MHV infection by arresting S-induced membrane fusion.

We exposed ^{35}S -labeled S1 dimers to the sulfhydryl alkylating agent *N*-ethylmaleimide (NEM) either before or after being complexed with N-CEACAM_{Fc} at 37 °C. In parallel, a monoclonal anti-S1₃₃₀ antibody (number 2) (25) was used in place of N-CEACAM_{Fc}, with the expectation that its binding would not induce conformational changes. Electropherograms of the immunoprecipitated ^{35}S -labeled proteins revealed that a small proportion of CEACAM-bound S1 had complexed into an ~220-kDa disulfide-linked protein (Fig. 8A, lane 4). Thiols apparently had to be available to generate the ~220-kDa protein, as S1 that had been pretreated with NEM bound N-CEACAM_{Fc} but did not couple into disulfide-linked oligomers (Fig. 8A, lane 3). Formation of the ~220-kDa protein required N-CEACAM_{Fc}, because mAb number 2 bound S1 but did not generate any electrophoretic mobility changes (Fig. 8B, lanes 3 and 4). Collectively, these data indicate that CEACAM binding can induce structural rearrangements in the S1 dimer, revealed in this experiment by alternative disulfide linkages.

Quaternary Structure of S2 Fragments after Separation from S1—High resolution structural data are available for portions

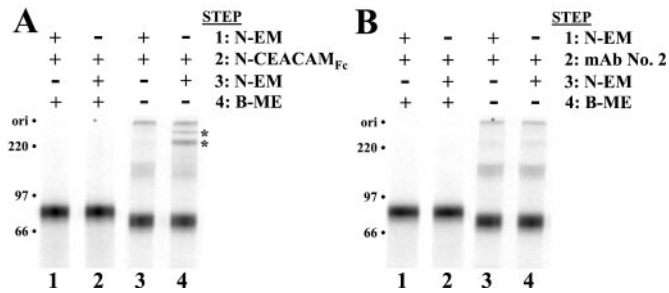


FIG. 8. **CEACAM-induced conformational changes in S1.** ^{35}S -Labeled $\text{S1}_{\Delta\text{DPR1}}$ was either incubated with (+) or without (-) 10 mM NEM prior to incubation for 4 h at 4 °C and then for 1 h at 37 °C with 10 μg of N-CEACAM_{FC} (A) or anti-S1₃₃₀ mAb number 2 (B) (25). Samples not previously treated with NEM were then incubated with 10 mM NEM (+). ^{35}S -Labeled proteins were detected by fluorography using a Molecular Dynamics Typhoon 8600 PhosphorImager following SDS-PAGE under reducing (+ B-ME) and non-reducing (- B-ME) conditions. N-CEACAM_{FC}-induced disulfide-linked high molecular weight spikes are indicated by the *.

of many different viral spike proteins, and the images reveal strong intersubunit interactions within integral membrane (fusion-inducing) post-translational fragments (6, 30–34, 36, 57). Less structural data are available for the peripheral (receptor binding) fragments, but collected information often leads to models in which these peripheral subunits separate from each other during membrane fusion reactions (36, 38). This “opening” of spike oligomers may expose hydrophobicity within the integral membrane fragments, a prerequisite for membrane fusion. Our discovery of stable intersubunit connections in coronavirus S1 led us to doubt whether these peripheral subunits separate during fusion, and also led us to speculate about additional oligomerization determinants in integral membrane S2 fragments.

We engineered S proteins with a relatively large 238-residue EGFP appended to their cytoplasmic tails. We found that the carboxyl-terminal additions had no effect on S protein transport through the exocytic pathway, indicating that oligomerization motifs in the S ectodomains remained. Moreover, S_{EGFP} proteins induced membrane fusion (data not shown). Therefore, these tagged S proteins allowed us to identify intersubunit associations through co-immunoprecipitation experiments. In one set of tests, we synthesized S and S_{EGFP} , either separately or together, in the presence of Tran^{35}S -label. We then immunoprecipitated all EGFP-tagged spikes from total cytoplasmic extracts using GFP-specific rabbit antiserum (a gift from Dr. Katherine L. Knight, Loyola University Medical Center), and we visualized S2 proteins by immunoblotting (Fig. 9A). Uncleaved S_{EGFP} and S2_{EGFP} were detected (lane 2), and when co-produced with S, the untagged S2 was also detected (lane 3). This association of S2_{EGFP} with untagged S2 was not due to a generalized aggregation of S2 chains after cell lysis, because there was no capture of S2 from mixtures of S and S_{EGFP} lysates (lane 4). The abundance of ^{35}S -labeled S1 in the immunoprecipitated material suggested that S1 dimers might be responsible for holding S2 and S2_{EGFP} together (Fig. 9B).

We next separated S1 dimers from S2 by tethering the spikes onto Sepharose:N-CEACAM_{FC} and then incubating at pH 8.5 and 37 °C. This condition separates S1 from S2 (58), leaving “free” S2 chains in supernatants. Sequential incubations with Sepharose:N-CEACAM_{FC} generated S1-depleted supernatants from which anti-GFP serum immunoprecipitated free S2 chains. Here there was capture of S2_{EGFP} (Fig. 9C, lanes 2 and 4), but there was no evidence of co-immunoprecipitating untagged S2 (lane 3). We correlated this co-immunoprecipitation failure with the absence of S1 in the samples (Fig. 9D). Collec-

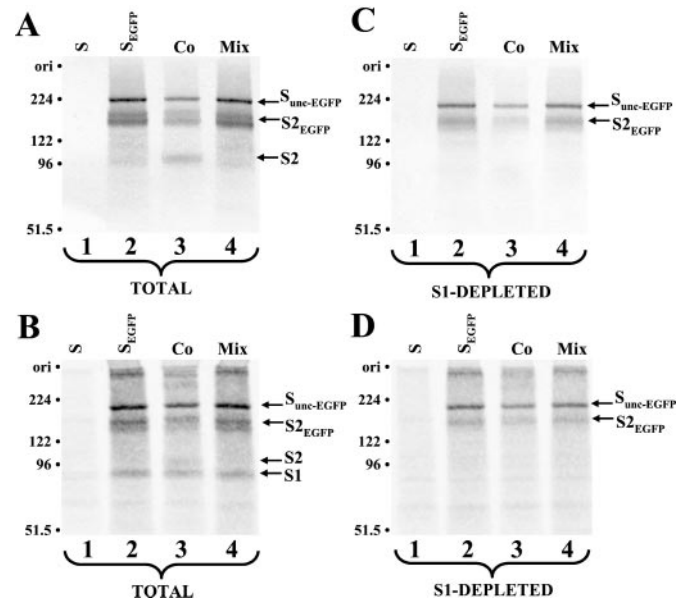


FIG. 9. **Analysis of the oligomeric organization of S2 after separation from S1.** A, cDNAs encoding S or EGFP-tagged S (S_{EGFP}) were transfected alone or together into vTF7.3-infected HeLa cells. Following metabolic labeling with Tran^{35}S -label, cytoplasmic extracts were prepared, and EGFP-associated proteins were immunoprecipitated with polyclonal anti-GFP serum. Immunoprecipitates were then electrophoresed and immunoblotted for S2 fragments. Co indicates co-synthesis of S and S_{EGFP} . Mix indicates that equal volumes of independently produced S and S_{EGFP} lysates were mixed before immunoprecipitation. B, autoradiographic image of the immunoblot in A. C, cell lysates were depleted of S1 by sequential immunoprecipitations with N-CEACAM_{FC} at pH 8.5 and 37 °C. Supernatants from the final depletions were collected, and EGFP-associated proteins were immunoprecipitated with anti-GFP serum. Immunoprecipitates were electrophoresed and immunoblotted for S2 fragments. D, autoradiographic image of the immunoblot in C. Arrows indicate the positions of uncleaved S_{EGFP} ($\text{S}_{\text{unc-EGFP}}$), S2_{EGFP} , untagged S2, and S1.

tively, these findings suggested that S2, when free of S1, does not exist as an oligomer.

DISCUSSION

The oligomeric spike glycoproteins of many enveloped viruses are endoproteolytically cleaved into two fragments that act in concert to mediate virion binding to receptors and subsequent uncoating through virion:cell membrane fusion. Crystal structures of the influenza hemagglutinin reveal an exterior composed of peripheral residues and their receptor-binding sites, and a core which harbors much of the integral membrane fragments, thereby sequestering the hydrophobic residues involved in membrane fusion. The dramatic conformational changes of integral membrane fragments that link opposing membranes can only be accomplished in concert with some displacement of the peripheral fragments. How this displacement process takes place remains unclear, *i.e.* whether the peripheral fragments symmetrically dissociate into monomers to reveal the membrane fusion apparatus, as depicted in some models (36, 38), or whether they displace asymmetrically as oligomers. We require additional insights into this process to understand the mechanisms by which antibodies neutralize virus infections and to develop chemicals that interfere with virus entry.

This issue of spike protein quaternary structures both before and after fusion activation has been studied in some detail with primate lentiviruses, and some interesting findings have emerged. The peripheral (gp120) fragments that shed from spike complexes during membrane fusion can be monomers, indeed they were crystallized in this form (54), but can also

exist as stable dimers (59–61) or trimers (62–64). By contrast, it is generally accepted that the integral membrane (gp41) fragments exist as trimers, at least in postfusion low energy conformations (29, 30, 32, 34, 65). Recent findings also indicate that different gp160 subunits, one with a lethal defect in receptor binding and the other unable to induce membrane fusion, can assemble together into functional heteromeric trimers (66). These findings naturally lead to the hypothesis that asymmetries can exist within gp120–41 complexes, at least in some of the conformations existent during fusion activation.

Similarly, it is conceivable that asymmetries exist in murine coronavirus spikes. We found that the peripheral (S1) fragments of MHV exist as stable, homogenous dimers (Fig. 1). Although we view our data as convincing, we understand its apparent inconsistency with previous reports of trimeric associations within MHV integral membrane (S2) fragments (67). Collective findings therefore raise the possibility that asymmetric dimer-to-trimer transitions occur as part of the pathway to membrane fusion activation. In this view, closely spaced S1 fragments would dissociate as stable dimers, leaving S2 fragments to rearrange during membrane fusion into trimeric structures. Such dimer-trimer transitions are not unprecedented in virus entry, although they take place in the context of icosahedrally ordered glycoprotein lattice (68, 69). No evidence exists for ordered arrangements of spikes on the pleiomorphic coronavirus envelopes.

Another interesting and potentially relevant asymmetry likely exists in S-CEACAM complexes. Only a single CEACAM binds to an S1 dimer. This was most convincingly demonstrated in our co-immunoprecipitation tests, where differentially tagged N-CEACAM fragments never captured S1-CEACAM complexes (Fig 6). Further support for a one S1 dimer:one CEACAM ratio came from our stoichiometric analyses of S1-N-CEACAM_{FC} complexes (Fig. 5). As we consider it unlikely that only a single asymmetric binding site exists on each S1 dimer (Fig. 7), we propose two alternative possibilities. Either the two CEACAM binding sites on an S1 dimer juxtapose very closely (steric hindrance) or the binding of a single CEACAM rapidly induces global structural changes in S1 that destroy the adjacent binding site (negative cooperativity). This latter possibility has received consideration in the SIV gp140-CD4 interaction, whose stoichiometry has recently been identified as an asymmetric complex of one gp140 trimer bound to a single monomeric CD4 (63). Our data, although not yet able to distinguish between the two possibilities, nonetheless provides evidence of structural flexibility in the S proteins and thus points toward negative cooperativity as a likely scenario. We and others know that CEACAM binding induces separation of S1 from S2, a readily observed “global” conformational change (23, 58). The CEACAM-binding site is itself dependent on a more global conformation, being formed with assembly of S into oligomers (Fig. 2), and eliminated on S1 dissociation into monomers (Fig. 3). This relationship between S oligomerization and CEACAM binding may provide the structural contexts for conformational changes across S1 monomers once a CEACAM molecule binds. In support of this view, we demonstrated that N-CEACAM_{FC} binding induced the formation of high molecular weight disulfide-linked S1 structures whose formation was blocked by pre-incubation with the sulfhydryl-alkylating agent N-ethylmaleimide (Fig. 8A). The inability of S1₃₃₀-specific mAb number 2 to induce comparable disulfide rearrangements (Fig. 8B) further supports the contention that entry-specific conformational changes in S1 are unique to CEACAM binding. Although these findings are interesting, perhaps even suggesting a role for disulfide exchanges during coronavirus entry (56), we acknowledge that additional CEACAM-induced changes in S1

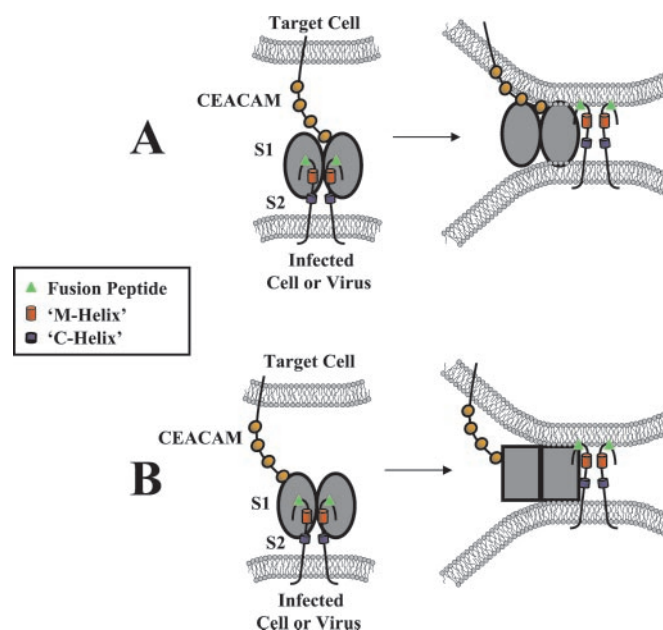


FIG. 10. Models depicting the quaternary structure of the MHV spike and its interaction with CEACAM during virus entry. To explain a single CEACAM-binding site on S1 dimers, two models are illustrated. Model A appeals to steric hindrance, and model B suggests that a single CEACAM induces global structural rearrangements (illustrated as the change of S1 from an oval to a rectangle). These conformational changes preclude additional CEACAM binding. In both cases, CEACAM binding is hypothesized to displace S1 from S2 (23) and to permit the insertion of an internal fusion peptide (green triangle) into the target cell membrane (71).

structure must be investigated to fully address how S conformations bring about virus:cell membrane fusion.

We were surprised to find oligomerization control in peripheral S1 fragments, because analogous viral glycoproteins oligomerize into trimers through interactions in their integral membrane fragments. Our attempts to determine whether the S1-interacting sites represent the only oligomerization motif prompted us to construct epitope-appended S proteins, and we discovered that tags as large as the 238-residue EGFP could be added to the carboxyl (cytoplasmic) termini of S2 without interrupting oligomeric assembly, intracellular transport, and function. With these epitope-tagged S proteins, it became relatively straightforward to determine whether S2 fragments retained an oligomeric structure even after separation from S1. Thus we bound soluble CEACAMs and shifted to 37 °C, a condition known to dissociate S1 from S2 (23). We expected that this would leave free S2 chains in an oligomeric state, as primary S2 sequences predict oligomeric coiled-coils (70) similar to those found in many other viral spike proteins that carry out membrane fusion reactions (29–34, 65). However, we did not co-immunoprecipitate S2-S2_{EGFP} complexes when free of S1, suggesting S2 monomers (Fig. 9). This interesting finding raises questions about the ways that MHV S2 might fuse membranes. The generally accepted view is that the integral membrane fragments of enveloped viruses collapse into α -helical coiled-coils on bringing opposing membranes together (36–41). It remains to be determined whether MHV S2 monomers independently adopt an anti-parallel α -helical coiled-coil arrangement that is similar to that observed for other viruses.

A preliminary model of S proteins during virus entry is shown in Fig. 10. In this figure, we depict a single CEACAM that is bound to peripheral S1 (25, 55). This bound CEACAM may preclude additional binding by steric hindrance (Fig. 10A) or alternatively may induce conformational changes in S1 oligomers that precludes additional CEACAM binding (Fig. 10B).

Additional conformational changes are thought to occur at S1-S2 connections, resulting in the displacement of the two fragments from each other (23). These events are considered prerequisites for the insertion of a hydrophobic portion of S2 into cellular membranes (71). As little is yet known regarding the later stages of the membrane fusion process, subsequent depictions of S2 structures are not illustrated. Coronavirus S2 fragments do contain putative M-helix and C-helix regions (Fig. 10), which are predicted to form coiled-coils (70). A collapse into coiled-coil structures may bring about membrane fusion in a fashion similar to that hypothesized for the enveloped myxoviruses (39), retroviruses (29, 30, 72), and filoviruses (33, 73). We intend to use this model to generate and refine hypotheses on coronavirus entry into cells.

Acknowledgments—We thank Sean Kelly for expert technical assistance and Edward Thorp, Dr. Alan J. Wolfe, and Dr. Joseph Brewer for critical reading of the manuscript.

REFERENCES

- Hernandez, L. D., Hoffman, L. R., Wolfsberg, T. G., and White, J. M. (1986) *Annu. Rev. Cell Dev. Biol.* **12**, 627–661
- Doranz, B. J., Baik, S. S. W., and Doms, R. W. (1999) *J. Virol.* **73**, 10346–10358
- Sattentau, Q. J., and Moore, J. P. (1991) *J. Exp. Med.* **174**, 407–415
- Wu, L., Gerard, N. P., Wyatt, R., Choe, H., Parolin, C., Ruffing, N., Borsetti, A., Cardoso, A. A., Desjardins, E., Newman, W., Gerard, C., and Sodroski, J. (1996) *Nature* **384**, 179–183
- Mothes, W., Boerger, A. L., Narayan, S., Cunningham, J. M., and Young, J. A. (2000) *Cell* **103**, 679–689
- Bullough, P. A., Hughson, F. M., Skehel, J. J., and Wiley, D. C. (1994) *Nature* **371**, 37–43
- Stegmann, T., White, J. M., and Helenius, A. (1990) *EMBO J.* **13**, 4231–4241
- Perlman, S., Lane, T. E., and Buchmeier, M. J. (2000) in *Effects of Microbes on the Immune System* (Cunningham, M., and Fujinami, R. S., eds) pp. 331–348, Lippincott-Raven, New York
- Sanchez, C. M., Izeta, A., Sanchez-Morgado, J. M., Alonso, S., Sola, I., Balasch, M., Plana-Duran, J., and Enjuanes, L. (1999) *J. Virol.* **73**, 7607–7618
- Phillips, J. J., Chua, M. M., Lavi, E., and Weiss, S. R. (1999) *J. Virol.* **73**, 7752–7760
- Kuo, L., Godeke, G. J., Raamsman, M. J., Masters, P. S., and Rottier, P. J. (2000) *J. Virol.* **74**, 1393–1406
- Schmidt, I., Skinner, M., and Siddell, S. G. (1987) *J. Gen. Virol.* **68**, 47–56
- Vennema, H., Rottier, P. J. M., Heijnen, L., Godeke, G. J., Horzinek, M. C., and Spaan, W. J. M. (1990) in *Coronavirus and Their Diseases* (Cananaugh, D., and Brown, T. D. K., eds) pp. 9–19, Plenum Publishing Corp., New York
- Sturman, L. S., Ricard, C. S., and Holmes, K. V. (1985) *J. Virol.* **56**, 904–911
- Frana, M. F., Behnke, J. N., Sturman, L. S., and Holmes, K. V. (1985) *J. Virol.* **56**, 912–920
- Yoo, D. W., Parker, M. D., and Babiuk, L. A. (1991) *Virology* **180**, 395–399
- Dveksler, G. S., Pensiero, M. N., Dieffenbach, C. W., Cardellicchio, C. B., Basile, A. A., Elia, P. E., and Holmes, K. V. (1993) *Proc. Natl. Acad. Sci. U. S. A.* **90**, 1716–1720
- Dveksler, G. S., Pensiero, M. N., Cardellicchio, C. B., Williams, R. K., Jiang, G.-S., Holmes, K. V., and Dieffenbach, C. W. (1991) *J. Virol.* **65**, 6881–6891
- Holmes, K. V., and Dveksler, G. S. (1994) in *Cellular Receptors for Animal Viruses* (Wimmer, E., ed) pp. 403–443, Cold Spring Harbor Laboratory Press, Cold Spring Harbor, NY
- Billker, O., Popp, A., Brinkmann, V., Wenig, G., Schneider, J., Caron, E., and Meyer, T. F. (2002) *EMBO J.* **21**, 560–571
- Leusch, H. G., Drzeniek, Z., Markos-Prustai, Z., and Wagener, C. (1991) *Infect. Immun.* **59**, 2051–2057
- Beauchemin, N., Draber, P., Dveksler, G., Gold, P., Gray-Owen, S., Hammarstrom, S., Holmes, K. V., Karlsson, A., Kuoriki, M., Lin, S.-H., Lucka, L., Najjar, S. M., Neumaier, M., Obrink, B., Shively, J. E., Skubit, K. M., Stanners, C. P., Thomas, P., Thompson, J. A., and Virji, M. A. (1999) *Exp. Cell Res.* **252**, 243–249
- Krueger, D. K., Kelly, S. M., Lewicki, D. N., Ruffolo, R., and Gallagher, T. M. (2001) *J. Virol.* **75**, 2792–2802
- Taguchi, F., and Matsuyama, S. (2002) *J. Virol.* **76**, 950–958
- Kubo, H., Yamada, Y. K., and Taguchi, F. (1994) *J. Virol.* **68**, 5403–5410
- Delmas, B., and Laude, H. (1990) *J. Virol.* **64**, 5367–5375
- Wilson, I. A., Skehel, J. J., and Wiley, D. C. (1981) *Nature* **289**, 366–373
- Wiley, D. C., and Skehel, J. J. (1987) *Annu. Rev. Biochem.* **56**, 365–394
- Weissenhorn, W., Wharton, S. A., Calder, L. J., Earl, P. L., Moss, B., Aliprandis, E., Skehel, J. J., and Wiley, D. C. (1996) *EMBO J.* **15**, 1507–1514
- Weissenhorn, W., Dessen, A., Harrison, S. C., Skehel, J. J., and Wiley, D. C. (1997) *Nature* **387**, 426–430
- Lu, M., Blacklow, S. C., and Kim, P. S. (1995) *Nat. Struct. Biol.* **2**, 1075–1082
- Bernstein, H. B., Tucker, S. P., Kar, S. R., McPherson, S. A., McPherson, D. T., Dubay, J. W., Lebowitz, J., Compans, R. W., and Hunter, E. (1995) *J. Virol.* **69**, 2745–2750
- Weissenhorn, W., Calder, L. J., Wharton, S. A., Skehel, J. J., and Wiley, D. C. (1998) *Proc. Natl. Acad. Sci. U. S. A.* **95**, 6032–6036
- Chan, D. C., Fass, D., Berger, J. M., and Kim, P. S. (1997) *Cell* **89**, 263–273
- Dutch, R. E., Leser, G. P., and Lamb, R. A. (1999) *Virology* **254**, 147–159
- Weissenhorn, W., Dessen, A., Calder, L. J., Harrison, S. C., Skehel, J. J., and Wiley, D. C. (1999) *Mol. Membr. Biol.* **16**, 3–9
- Skehel, J. J., and Wiley, D. C. (1998) *Cell* **95**, 871–874
- Eckert, D. M., and Kim, P. S. (2001) *Annu. Rev. Biochem.* **70**, 777–810
- Joshi, S. B., Dutch, R. E., and Lamb, R. A. (1998) *Virology* **248**, 20–34
- Melikyan, G. B., Markosyan, R. M., Hemmati, H., Delmedico, M. K., Lambert, D. M., and Cohen, F. S. (2000) *J. Cell Biol.* **151**, 413–423
- Russell, C. J., Jardetzky, T. S., and Lamb, R. A. (2001) *EMBO J.* **20**, 4024–4034
- Gallagher, T. M. (1997) *J. Virol.* **71**, 3129–3137
- Parker, S. E., Gallagher, T. M., and Buchmeier, M. J. (1989) *Virology* **173**, 664–673
- Mackett, M., Smith, G. L., and Moss, B. (1984) *J. Virol.* **49**, 857–864
- Fuerst, T. R., Earl, P. L., and Moss, B. (1987) *Mol. Cell. Biol.* **7**, 2538–2544
- Fleming, J. O., Stohlman, S. A., Harmon, R. C., Lai, M. M. C., Frelinger, J. A., and Werner, L. P. (1983) *Virology* **131**, 296–307
- Routledge, E., Stauber, R., Pfeleiderer, M., and Siddell, S. G. (1991) *J. Virol.* **65**, 254–262
- Young, B. D. (1984) in *Centrifugation: A Practical Approach* (Rickwood, D., ed) 2nd Ed., pp. 127–140, IRL Press, Washington D. C.
- Cavanagh, D. (1995) in *The Coronaviridae* (Siddell, S. G., ed) pp. 73–103, Plenum Publishing Corp., New York
- Doms, R. W., Lamb, R. A., Rose, J. K., and Helenius, A. (1993) *Virology* **19**, 545–562
- Tatu, U., Hammond, C., and Helenius, A. (1995) *EMBO J.* **14**, 1340–1348
- Feldmann, H., Will, C., Schikore, M., Slenczka, W., and Klenk, H. D. (1991) *Virology* **182**, 353–356
- Sattentau, Q. J., Moore, J. P., Vignaux, F., Traincard, F., and Poignard, P. (1993) *J. Virol.* **67**, 7383–7393
- Kwong, P. D., Wyatt, R., Robinson, J., Sweet, R. W., Sodroski, J., and Hendrickson, W. A. (1998) *Nature* **393**, 648–659
- Suzuki, H., and Taguchi, F. (1996) *J. Virol.* **70**, 2632–2636
- Gallagher, T. M. (1996) *J. Virol.* **70**, 4683–4690
- Chen, J., Wharton, S. A., Weissenhorn, W., Calder, L. J., Hughson, F. M., Skehel, J. J., and Wiley, D. C. (1995) *Proc. Natl. Acad. Sci. U. S. A.* **92**, 12205–12209
- Sturman, L. S., Ricard, C. S., and Holmes, K. V. (1990) *J. Virol.* **64**, 3042–3050
- Doms, R. W., Earl, P. L., and Moss, B. (1991) *Adv. Exp. Med. Biol.* **300**, 203–219
- Earl, P. L., Doms, R. W., and Moss, B. (1992) *J. Virol.* **66**, 5610–5614
- Center, R. J., Earl, P. L., Lebowitz, J., Schuck, P., and Moss, B. (2000) *J. Virol.* **74**, 4448–4455
- Earl, P. L., Doms, R. W., and Moss, B. (1990) *Proc. Natl. Acad. Sci. U. S. A.* **87**, 648–652
- Kim, M., Chen, B., Hussey, R. E., Chishti, Y., Montefiori, D., Hoxie, J. A., Byron, O., Campbell, G., Harrison, S. C., and Reinherz, E. L. (2001) *J. Biol. Chem.* **276**, 42667–42676
- Center, R. J., Schuck, P., Leapman, R. D., Arthur, L. O., Earl, P. L., Moss, B., and Lebowitz, J. (2001) *Proc. Natl. Acad. Sci. U. S. A.* **98**, 14877–14882
- Weissenhorn, W., Calder, L. J., Dessen, A., Laue, T., Skehel, J. J., and Wiley, D. C. (1997) *Proc. Natl. Acad. Sci. U. S. A.* **94**, 6065–6069
- Salzwedel, K., and Berger, E. A. (2000) *Proc. Natl. Acad. Sci. U. S. A.* **97**, 12794–12799
- Gallagher, T. M., Parker, S. E., and Buchmeier, M. J. (1990) *J. Virol.* **64**, 731–741
- Lescar, J., Roussel, A., Wien, M. W., Navaza, J., Fuller, S. D., Wengler, G., Wengler, G., and Rey, F. A. (2001) *Cell* **105**, 137–148
- Pletnev, S. V., Zhang, W., Mukhopadhyay, S., Fisher, B. R., Hernandez, R., Brown, D. T., Baker, T. S., Rossmann, M. G., and Kuhn, R. J. (2001) *Cell* **105**, 127–136
- Singh, M., Berger, B., and Kim, P. S. (1999) *J. Mol. Biol.* **290**, 1031–1041
- Luo, Z., and Weiss, S. R. (1998) *Virology* **244**, 483–494
- Fass, D., Davey, R. A., Hamson, C. A., Kim, P. S., Cunningham, J. M., and Berger, J. M. (1997) *Science* **277**, 1662–1666
- Gallagher, W. R. (1996) *Cell* **85**, 477–478

PROTEIN STRUCTURE AND FOLDING:
**Quaternary Structure of Coronavirus
Spikes in Complex with Carcinoembryonic
Antigen-related Cell Adhesion Molecule
Cellular Receptors**

Daniel N. Lewicki and Thomas M. Gallagher
J. Biol. Chem. 2002, 277:19727-19734.

doi: 10.1074/jbc.M201837200 originally published online March 23, 2002

Access the most updated version of this article at doi: [10.1074/jbc.M201837200](https://doi.org/10.1074/jbc.M201837200)

Find articles, minireviews, Reflections and Classics on similar topics on the [JBC Affinity Sites](https://www.jbc.org/affinity-sites).

Alerts:

- [When this article is cited](#)
- [When a correction for this article is posted](#)

[Click here](#) to choose from all of JBC's e-mail alerts

This article cites 68 references, 38 of which can be accessed free at
<http://www.jbc.org/content/277/22/19727.full.html#ref-list-1>